ADVANCED MATERIALS
www.advmat.de

Effect of Adventitious Carbon on Pit Formation of Monolayer MoS_2

*Sangwook Park, Samira Siahrostami, Joonsuk Park, Amir Hassan Bagherzadeh Mostaghimi, Taeho Roy Kim, Lauren Vallez, Thomas Mark Gill, Woosung Park, Kenneth E. Goodson, Robert Sinclair, and Xiaolin Zheng**

Forming pits on molybdenum disulfide (MoS_2) monolayers is desirable for (opto)electrical, catalytic, and biological applications. Thermal oxidation is a potentially scalable method to generate pits on monolayer MoS_2, and pits are assumed to preferentially form around undercoordinated sites, such as sulfur vacancies. However, studies on thermal oxidation of MoS_2 monolayers have not considered the effect of adventitious carbon (C) that is ubiquitous and interacts with oxygen at elevated temperatures. Herein, the effect of adventitious C on the pit formation on MoS_2 monolayers during thermal oxidation is studied. The in situ environmental transmission electron microscopy measurements herein show that pit formation is preferentially initiated at the interface between adventitious C nanoparticles and MoS_2, rather than only sulfur vacancies. Density functional theory (DFT) calculations reveal that the C/MoS_2 interface favors the sequential adsorption of oxygen atoms with facile kinetics. These results illustrate the important role of adventitious C on pit formation on monolayer MoS_2.

To date, the thermal oxidation of 2H phase MoS_2 monolayers have been investigated through many spectroscopic and microscopic characterization techniques (e.g., X-ray photoelectron spectroscopy (XPS),[1] Raman spectroscopy,[2] atomic force microscopy (AFM),[1–4] and scanning electron microscopy (SEM)[4]), and density functional theory (DFT) calculations.[5–7] The oxidized MoS_2 monolayers frequently have pits due to the formation of volatile MoO_3 and gaseous SO_2 and SO_3.[1–4] These defects are often observed near edges and grain boundaries of MoS_2, where the stronger oxidative tendency is attributed to the presence of a higher concentration of undercoordinated sites.[7,8] DFT calculations also revealed that sulfur vacancies are prone to be occupied by atomic oxygen.[5,6] Nevertheless, all these previous studies on the pit formation of MoS_2 monolayers by thermal oxidation have not considered the effects of adventitious carbon (C), which is ubiquitous and nearly impossible to fully remove. Adventitious C is even more pronounced under vacuum conditions, such as those conditions used for chemical vapor deposition synthesis of MoS_2 and microscope characterization environments. On the other hand, carbon is known to adsorb and catalyze the dissociation of oxygen (O_2)[9–11] and moisture (H_2O),[12,13] so such interactions can potentially affect the oxidation process of the MoS_2 monolayers. However, the role of adventitious C on the oxidation process of MoS_2 monolayers has not been reported.

Herein, we combine in situ environmental transmission electron microscopy (ETEM) under an O_2 environment and DFT calculation for the adsorption energy of oxygen atoms on different sites in the monolayer MoS_2 to study the pit formation mechanism of a monolayer MoS_2 by thermal oxidation at the atomic level in the presence of adventitious carbon. It should be noted that in situ TEM has been used to investigate the phase transition between 2H and 1T phases,[14] crack[15] and pit[16] formation, and atom[16,17] and sulfur vacancy[18] migration in MoS_2 monolayers without the presence of gas. However, there is no reported in situ TEM characterization of a monolayer MoS_2 at the atomic level in the presence of gases. Similar in situ TEM studies of reactions between solid materials and gases often use a specialized holder with a window cell that has a pair of electron transparent membranes (e.g., SiN_x, tens of nanometers thick) to seal the samples in between. These window cells have been successfully used to study the reaction between nanoparticles (e.g., Rh,[19] Pt-Ni,[20] and Cu_2O/Cu[21]) and gases (e.g., O_2,[20,21]

Dr. S. Park, L. Vallez, T. M. Gill, Prof. K. E. Goodson, Prof. X. Zheng
Department of Mechanical Engineering
Stanford University
440 Escondido Mall, Stanford, CA 94305, USA
E-mail: xlzheng@stanford.edu
Prof. S. Siahrostami, A. H. B. Mostaghimi
Department of Chemistry
University of Calgary
2500 University Drive NW, Calgary, Alberta T2N 1N4, Canada
Dr. J. Park, Prof. R. Sinclair
Department of Materials Science and Engineering
Stanford University
496 Lomita Mall, Stanford, CA 94305, USA
Dr. T. R. Kim
Stanford Nano Shared Facilities
Stanford University
476 Lomita Mall, Stanford, CA 94305, USA
Prof. W. Park
Department of Mechanical Systems Engineering
Sookmyung Women's University
Seoul 04310, South Korea
The ORCID identification number(s) for the author(s) of this article can be found under https://doi.org/10.1002/adma.202003020.

DOI: 10.1002/adma.202003020

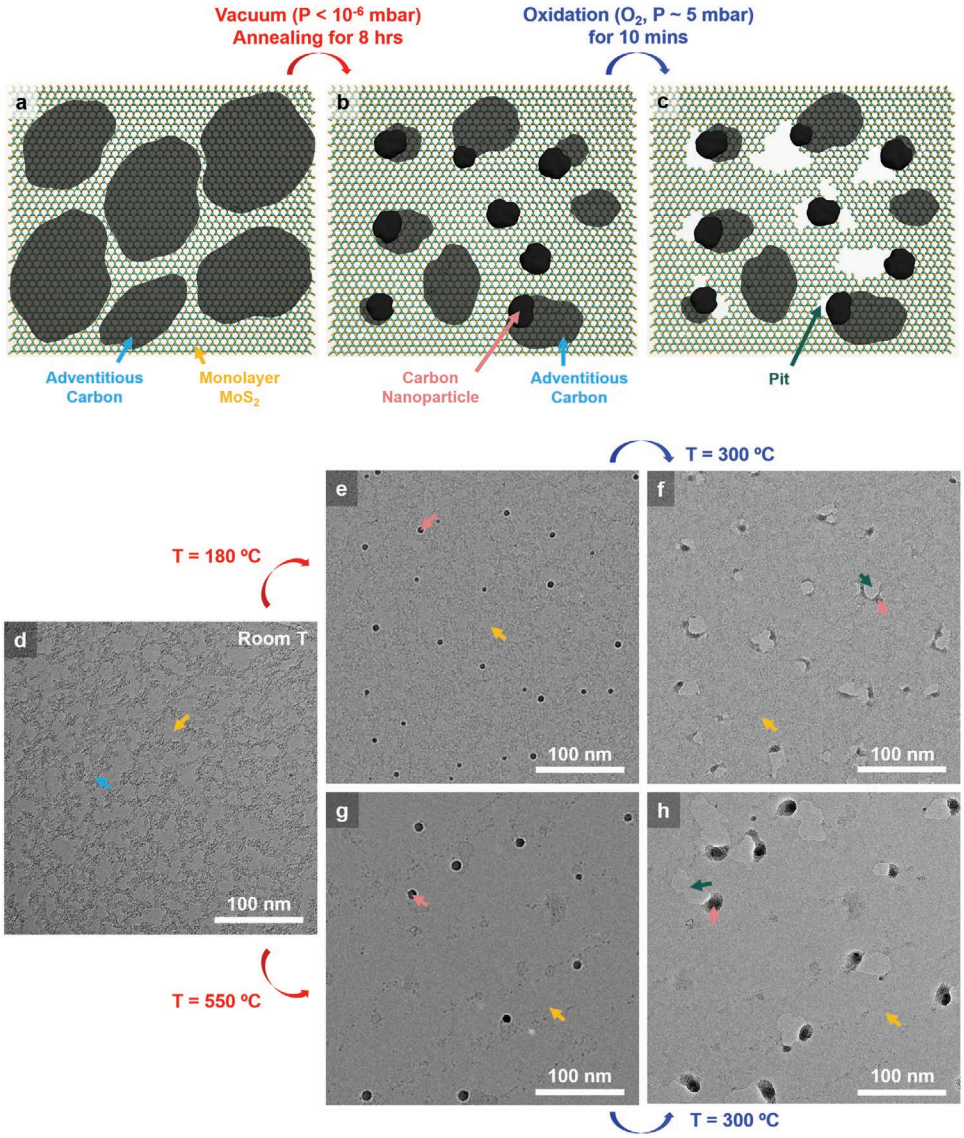

Figure 1. Schematic and aberration-corrected TEM images of MoS_2 monolayers basal plane (top view). a) Schematic and d) TEM image of pristine MoS_2 monolayers (orange arrow) with floating adventitious C (light blue arrow). b) Schematic and e,g) TEM images (e.g., 180 °C and 550 °C, respectively) of vacuum annealed monolayer MoS_2 at high temperature with dark gray agglomerated C nanoparticles (pink arrow) and light gray adventitious C (light blue arrow; (b)). c) Schematic and f,h) TEM images of oxidized monolayer MoS_2 with etched pits (green arrow) right adjacent to the agglomerated C nanoparticles.

H_2,[19–21] N_2,[19,20] CO,[20] and CO_2[19]). However, these window cells are not ideal for studying ultrathin samples, such as MoS_2 monolayers, because the membranes scatter the electron beam and reduce the intrinsic instrumental spatial resolution. Such effects are more pronounced for imaging ultrathin MoS_2 monolayers (≈0.65 nm thick[22]) because of low electron acceleration voltage (≤80 kV) and beam dose (≤10^4 e^- $Å^{-2}$ s^{-1}) are used to prevent the monolayers from electron beam damage. Instead, we used an aperture type ETEM (Titan 80–300)[23,24] and an 80 kV operating voltage to study the reaction between MoS_2 monolayers and O_2 in situ.

Figure 1 shows the schematic and aberration-corrected TEM images of MoS_2 monolayers at three different stages of the in situ ETEM measurement (see Supporting Information for details). First, before any annealing, the as-grown monolayer MoS_2 is covered by adventitious C (Figure 1a,d). The chemical identity of the adventitious C is confirmed by XPS, which shows a characteristic C—C peak at ≈284.8 eV (Figure S1, Supporting Information). Others also observed a similar prevalence of adventitious C on MoS_2 monolayers.[14,17] Under e-beam irradiation, we observed that the adventitious C moves around on the monolayer MoS_2 (Movies S1, S2, and Figure S2, Supporting Information), indicating that the interaction between C and MoS_2 is weak likely through van der Waals (vdW) forces.[17] Second, after high-temperature vacuum annealing without an electron beam, some adventitious C agglomerates into C nanoparticles to minimize its surface energy, which consequently enlarges the area of clean MoS_2 surface (Figure 1b,e,g). The TEM

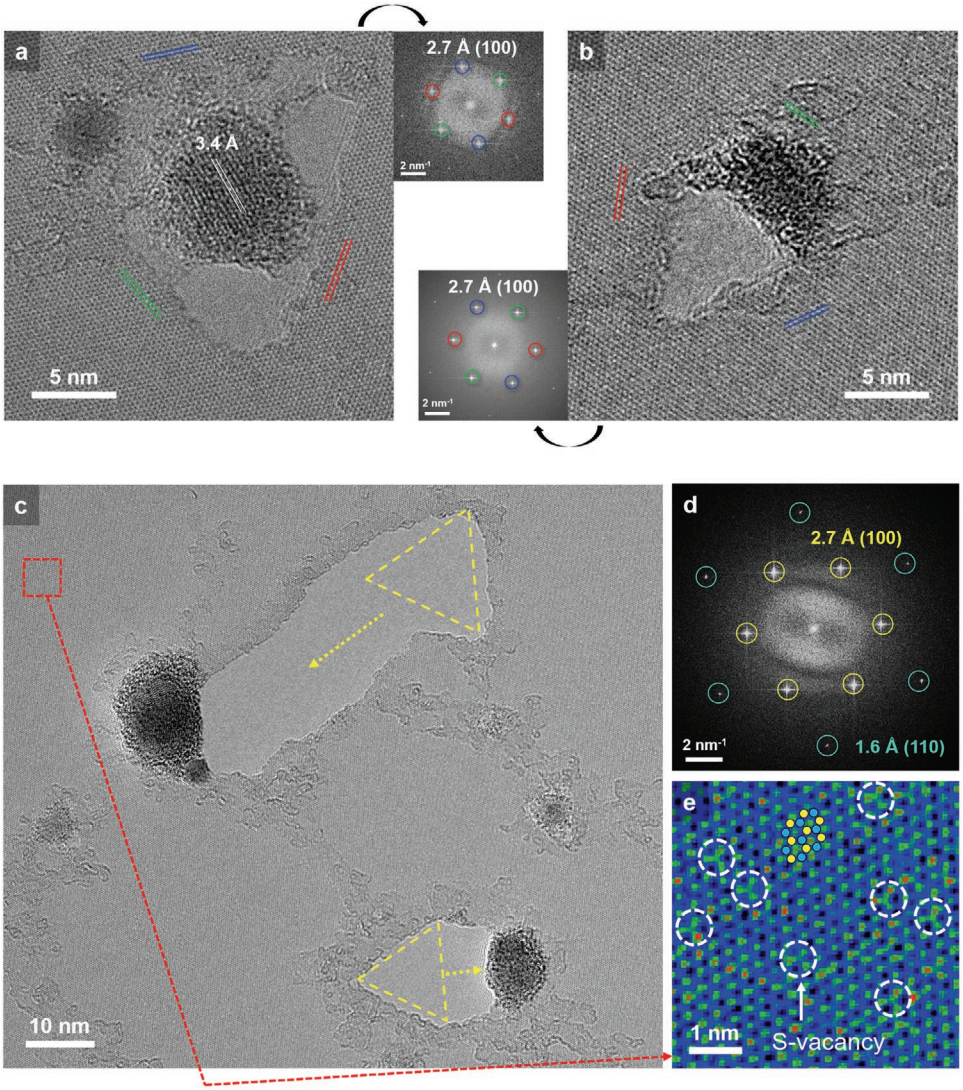

Figure 2. Aberration-corrected high-resolution TEM images of the oxidized single crystalline MoS_2 monolayers. a,b) Agglomerated C nanoparticle centered in (a) and on the edge of (b) a triangular pit. The corresponding FFT of the monolayer MoS_2 is located on the top right (a) and bottom left (b) side of the TEM images. The red, blue, and green lines on the lattice fringe of TEM images correspond to the same colored circles in the corresponding FFT image. c) Agglomerated C nanoparticles, long pits, and S-vacancies exist on the basal plane of the monolayer MoS_2 after oxidation. d) FFT image of the monolayer MoS_2 in (c). e) Magnified false-color TEM image of S-vacancies on the basal plane of a monolayer MoS_2 from the red dashed square window in (c). The corresponding positions of Mo (blue circle) and S (yellow circle) atoms are partially marked. All the samples were annealed at 180 °C and $P < 10^{-6}$ mbar for 8 h, and oxidized at 300 °C and $P \approx 5$ mbar (O_2) for 10 min.

images show continuous MoS_2 film (no pits) covered by adventitious C before thermal oxidation. We tested two annealing temperatures of 180 °C (Figure 1e) and 550 °C (Figure 1g) and found that a higher annealing temperature leads to larger and fewer C nanoparticles (Figure S3a, Supporting Information, 180 °C, number density: 129 particles per μm^2, projected area per particle: 30 nm^2; 550 °C: 24 particles per μm^2, 116 nm^2). These C nanoparticles show lattice fringes of 2.0, 2.1, and 3.4 Å in **Figure 2**a and Figure S4, Supporting Information, matching the (101), (100), and (002) planes of graphitic carbon (JCPDS, #56-0159). It is challenging to tell if those C nanoparticles are partially organic or not in nature. However, our DFT calculation illustrates that hydrocarbon is unlikely to contribute to the surface oxidation of monolayer MoS_2 since hydrocarbon strongly absorbs oxygen atom (ΔE_0 = –4.13 eV) and desorbs from the MoS_2 surface (Figure S5, Supporting Information). Hence, we assume that only pure C nanoparticles are important here. Finally, after the monolayer MoS_2 was exposed to O_2 (≈5 mbar) at 300 °C for 10 min without an electron beam, we observed that pits (or holes), an indication of MoS_2 oxidation, are formed around the C nanoparticles (Figure 1c,f,h). The sizes of the pits are larger around the larger C nanoparticles. It should be noted that we did not image the monolayer MoS_2 during the oxidation process in the presence of O_2, because the ionized oxygen beam damages the monolayer MoS_2 (Figure S6, Supporting Information).

Next, we zoomed in to inspect the relationship between C nanoparticles and pits using the aberration-corrected high-resolution TEM (see Supporting Information for details).

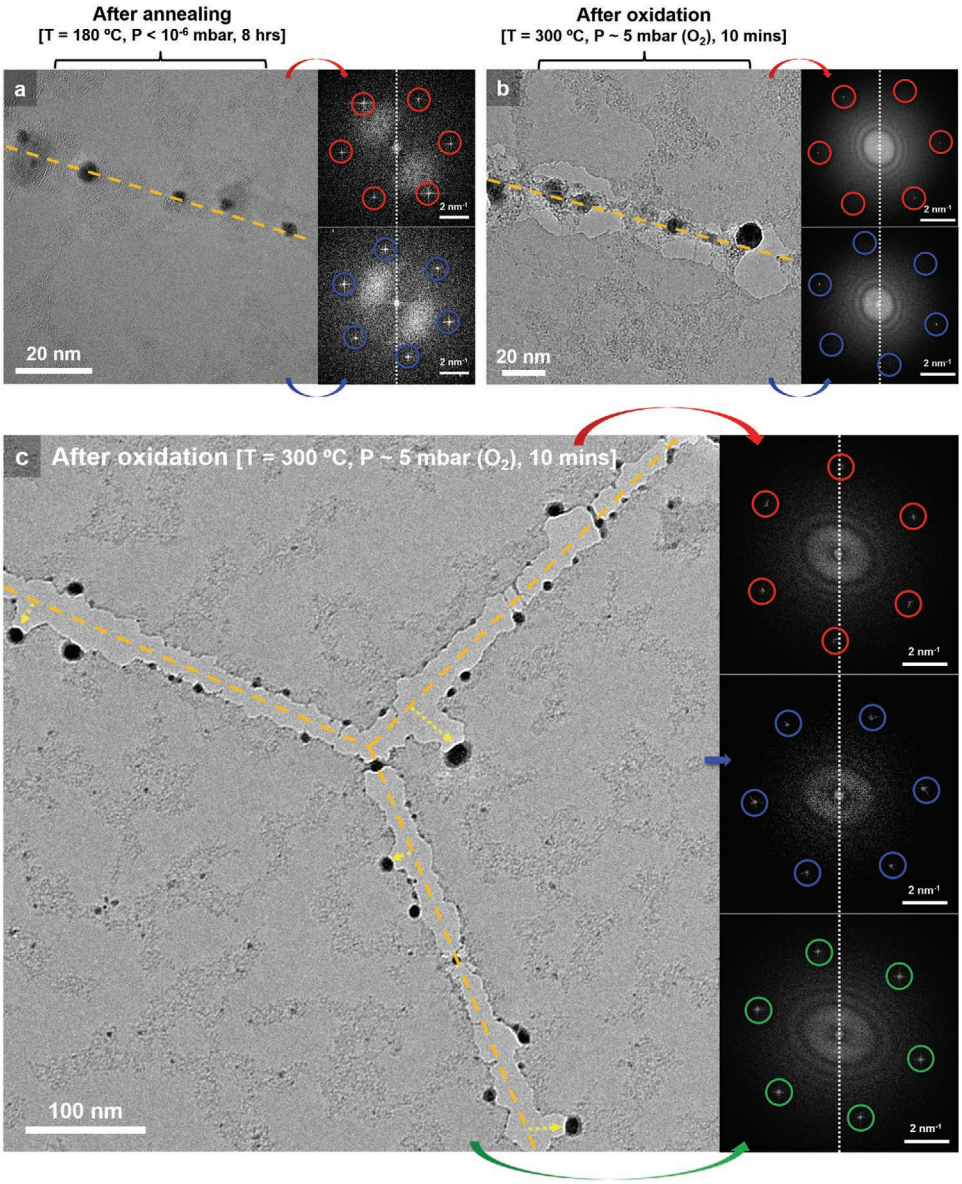

Figure 3. Aberration-corrected high-resolution TEM images of grain boundaries of polycrystalline MoS_2 monolayers. a) Agglomerated C nanoparticles align along a grain boundary (orange dash line) of a monolayer MoS_2 after annealing. b) Formation of pits by oxidation initiates right adjacent to the C nanoparticles on the grain boundary (orange dash line) of a monolayer MoS_2. c) Pits propagate and form gaps along the grain boundaries (orange dash lines) of a monolayer MoS_2 by oxidation. Long pits (yellow dot arrows) are also generated from the grain boundary and right adjacent to the C nanoparticles after oxidation. The corresponding FFT images show grain domains on different sides of the orange dash lines, where the different orientations of every single crystalline grain of the monolayer MoS_2 marked with the same colored arrows and circles (red, blue, or green).

We studied C nanoparticles at two representative positions of the monolayer MoS_2: one on the single-crystalline domains (Figure 2) and the other on the grain boundaries (**Figure 3**). When C nanoparticles are on the single crystalline domain of MoS_2, we observed three types of pits: several small pits (2–7 nm) surrounding a C nanoparticle (Figure 2a), a triangular shape pit sharing an edge with a C nanoparticle (Figure 2b), and a long pit sharing an edge with a C nanoparticle (Figure 2c). Some edges of those pits approximately align with the (100) planes of MoS_2, which are marked as the red, blue, and green parallel lines in Figure 2a,b. Some pits propagate into irregular shapes as the oxidation progresses and the C nanoparticles move (Figure 2c, Movies S8–S10, and Figure S7i–l, Supporting Information). The (100) planes are confirmed by both the aberration-corrected high-resolution TEM images and the fast Fourier transform (FFT) that shows a lattice constant of 2.7 Å, matching the *d*-spacing of (100) planes in MoS_2 (JCPDS #37-1492).[25,26] The long pit in Figure 2c has one end bordering with the C nanoparticle, and the other end appears to be triangular with edges parallel to the (100) planes (yellow dot triangles) of MoS_2 (FFT is shown in Figure 2d). The formation of this long pit appears to start at the yellow dot triangle region, and then the weakly bonded C nanoparticle most likely moves away while promoting the oxidation along its path, forming the long pit.

Similar triangular pits with (100) edges are frequently observed for oxidized MoS_2[2,7] because the (100) planes of MoS_2 have the lowest energy thermodynamically.[27,28] Hence, the shapes of the pits are determined largely by their thermodynamic energy, rather than the initiation mechanism that is dictated by the location of the pits. Importantly, no pit formation is observed on the clean parts of MoS_2 (Figure 2c, red dot square window), which contain many intrinsic S-vacancies that were possibly created from the synthesis and transfer processes of MoS_2 monolayers for the TEM sample preparation (Figure 2e and Figure S8a,b, white dot circles; Table S1, Supporting Information). Figure 2e and Figure S8a,b, Supporting Information, are false-color aberration-corrected high-resolution TEM images, which makes S-vacancies (green color) more visible from the bluish background of the original S atom positions.[29] These results show that the interfaces between C nanoparticles and MoS_2 are more preferred sites than only S-vacancies for pit formation. The similar dynamics of pit formations on MoS_2 monolayers was also observed in the presence of O_2 gas using a low electron dose rate of 100 e^- $Å^{-2}$ s^{-1} (Movies S3–S10 and Figure S7, Supporting Information).

We further examined the scenarios when C nanoparticles are located at the grain boundaries of the MoS_2 monolayers. We observed a similar phenomenon of pits forming only around C nanoparticles (Figure 3). After vacuum annealing (180 °C, 8 h), many C nanoparticles are aligned in nearly straight lines as shown in Figure 3a (see larger area TEM images in Figure S9a, Supporting Information). The FFT analysis in Figure 3a shows that those lines correspond to grain boundaries because two sides of the line exhibit different crystal orientations. The grain

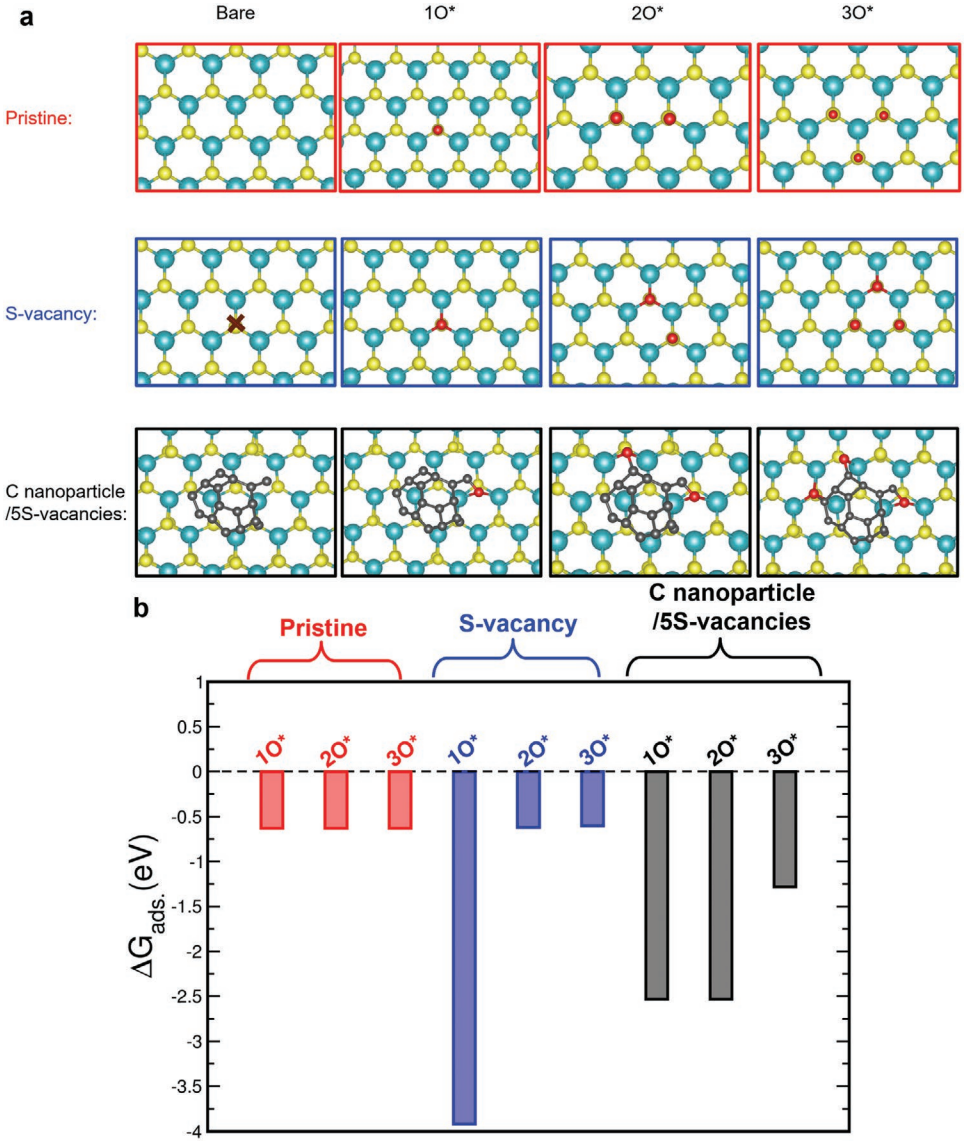

Figure 4. DFT calculation of three sequential oxygen atoms adsorption energy for three different model structures. a) Model structures of pristine (red), S-vacancy (blue), and C nanoparticle on 5S-vacancies (black) of MoS_2 monolayer basal plane are described in the first column, respectively. The sequential three oxygen atom adsorptions (1O*, 2O*, and 3O*) in each model structure are described in a row. Color code: S, yellow; Mo, cyan; C, gray; O, red. b) The adsorption energy of three oxygen atoms for progressive oxidation in each model structure shown in (a) is calculated.

boundaries of MoS_2 monolayers contain many undercoordinated sites[28,30,31] and the calculated diffusion barrier for C nanoparticles is ≈4.7 eV on undercoordinated sites, such as S-vacancy. Hence, once C nanoparticles diffuse to the grain boundaries, they are trapped and align along these grain boundaries in straight lines. After exposing MoS_2 to the oxidation condition (300 °C, 10 min, and ≈5 mbar of O_2), again, pits are formed around those C nanoparticles (Figure 3b, see larger area TEM images in Figure S10, Supporting Information). Those pits connect and form straight gaps across the grain boundaries (Figure 3c), and the C nanoparticles have migrated from the grain boundaries to the two edges of the gaps. A few branched pits are also observed adjacent to the grain boundary (Figure 3c, yellow dot arrows) and they are likely caused by the movement of the C nanoparticles, like the long pit in Figure 2c. Also, we did not observe any pit formation when exposing the monolayer MoS_2 to 300 °C without O_2 (Figure S9b, Supporting Information), confirming that pit formation is associated with the oxidation process. In short, the TEM images in Figures 1-3 show that pits (i.e., oxidation of MoS_2) are preferentially formed around C nanoparticles, regardless of their locations. Besides, the C nanoparticles are mobile on the surface of the MoS_2 and their movement leads to elongated pits.

We further carried out DFT calculations using the climbing image nudged elastic band (CI-NEB) method to compare the oxygen adsorption behavior on different sites to understand the role of C nanoparticles on pit formation. Of note, our DFT calculations show that the physisorbed C nanoparticles on MoS_2 have a negligible diffusion barrier, which supports the experimentally observed movement of adventitious C. However, when carbon clusters are trapped in the S-vacancies of the basal plane of the monolayer MoS_2, they have a very high diffusion barrier ≈4.7 eV. This suggests that carbon impurities tend to agglomerate in the S-vacancies.

Figure S11b, Supporting Information, compares the oxidation tendency of adsorbing a single oxygen atom on nine different sites on MoS_2 (see Supporting Information for details). Experimentally observed MoS_2 oxidation, or pit formation, involves adsorption of multiple oxygen atoms, so we further calculated the oxygen adsorption energy for successive addition of atomic oxygen up to three; 1O*, 2O*, and 3O*. Due to the high computational cost, we considered three structures (**Figure 4**a): pristine MoS_2 as a reference, a single S-vacancy on the basal plane, and a C nanoparticle supported on five S-vacancies. The latter two structures were shown to strongly adsorb a single oxygen atom (Figure S11b, Supporting Information). Figure 4b plots the sequential oxygen adsorption energy on these three model structures. First, we found that none of the three oxygen atoms bind strongly to pristine MoS_2 ($\Delta G_{ads.} \approx -0.5$ eV), indicating unfavorable oxidation. Second, for the single S-vacancy, the first oxygen atom is strongly adsorbed, but the subsequent adsorption of the second and third oxygen becomes significantly less favorable with adsorption energies ≈ −0.5 eV. This suggests that a single S-vacancy can be easily filled by oxygen, but it also inhibits further oxidation. Third, when a C nanoparticle is present, all three oxygen atoms show strong adsorption at the interface between C nanoparticle and MoS_2 ($\Delta G_{ads.}$ of −2.5 eV, −2.5 eV, and −1.25 eV), which is about ten times stronger than that on the C nanoparticles (Figure S12, Supporting Information, ΔE_o: −0.21 to 1.50 eV). These DFT results also suggest that progressive oxidation is thermodynamically more favorable when C nanoparticles are present. Also, the calculated potential energy diagram shows that O_2 dissociation is barrierless and downhill at the interface between C nanoparticle and monolayer MoS_2 (Figure S13, Supporting Information). This indicates the facile oxidation process in the interface of the C nanoparticle and MoS_2 substrate. Finally, the experimental observations and theoretical calculations suggest the following oxidation mechanism of monolayer MoS_2 (see Supporting Information for details). The oxidation is initiated at the interface between C nanoparticle and MoS_2, which forms gaseous SO_x and solid MoO_x. SO_x leaves and MoO_x moves, forming pits on MoS_2 monolayers. MoO_x is difficult to observe in TEM due to its sensitivity to the electron beam[32] but the formation of MoO_x was confirmed by SEM, Auger electron spectroscopy (AES), and XPS analysis of ex situ thermal oxidation of MoS_2 monolayers (Figure S14, Supporting Information).

Last, we demonstrated the application of MoS_2 monolayers with pits as electrocatalysts for hydrogen evolution reaction

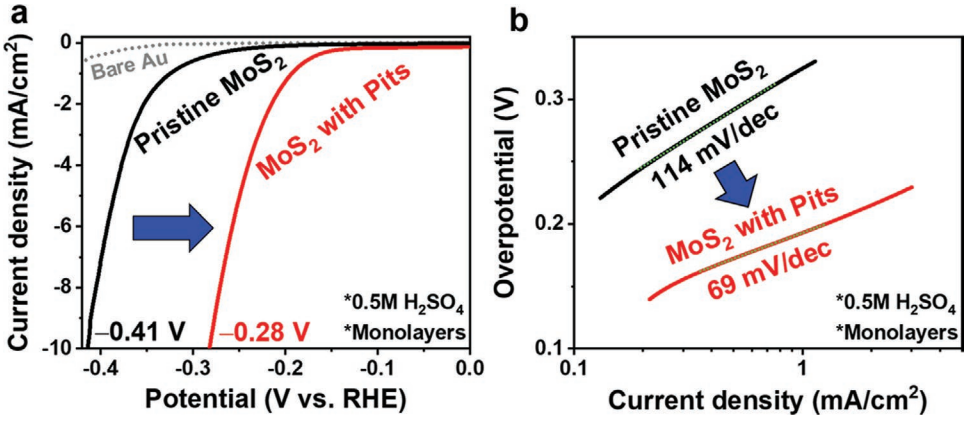

Figure 5. Comparisons of HER activity between the pristine monolayer MoS_2 and monolayer MoS_2 with pits. a) Linear sweep voltammograms (LSV). b) Corresponding Tafel plots of the polarization curves in (a). Electrolyte: 0.5 M H_2SO_4. For both cases, MoS_2 monolayers were supported on Au-coated Si wafers. The pits were formed on monolayer MoS_2 samples by sequential thermal annealing under Ar at 1 atm at 180 °C for 8 h, and at 300 °C for 10 min under the O_2 partial pressure of ≈5 mbar with the Ar balance.

(HER). The formed pits on MoS_2 contain active edge sites for HER[33] and thus HER activity of MoS_2 should increase after pit formation, which is supported by our experimental data shown in **Figure 5**.

In summary, we conducted the first in situ ETEM study on the pit formation process of MoS_2 monolayers by thermal oxidation. We found that MoS_2 monolayers unavoidably contain adventitious C and it agglomerates into C nanoparticle under annealing conditions. Our experiments show that the oxidized MoS_2 monolayers contain pseudo-triangular shaped pits. Those pits prefer to form at the interface between C nanoparticles and MoS_2 monolayers, rather than at other places, including single S-vacancy sites. Our DFT results show that a single S-vacancy can be easily filled by oxygen that inhibits its further oxidation. Instead, when a C nanoparticle is present on the monolayer MoS_2, progressive oxidation is thermodynamically favorable, which supports our experimental results. Our results illustrate the importance of adventitious C on promoting the pit formation of a monolayer MoS_2 by thermal oxidation. These results suggest that controlling the amount of adventitious C, perhaps other impurities as well, on MoS_2 monolayers and other ultrathin materials, will facilitate the pit formation for their diverse applications such in electronics,[2,34,35] catalysis,[7,33] and biology.[36]

Supporting Information

Supporting Information is available from the Wiley Online Library or from the author.

Acknowledgements

S.P., S.S., and J.P. contributed equally to this work. X.Z. acknowledges generous financial support from Stanford SystemX Alliance and Stanford Precourt Institute for Energy. S.P. acknowledges the generous financial support from the Kwanjeong Educational Foundation. S.S. and A.H.B.M. acknowledge the support from the University of Calgary's Canada First Research Excellence Fund Program, the Global Research Initiative in Sustainable Low Carbon Unconventional Resources. Part of the research at Sookmyung Women's University was supported by the National Research Foundation of Korea (NRF-2018R1C1B5086589). Part of this work (TEM, XPS, and Raman spectroscopy) was performed at Stanford Nano Shared Facilities (SNSF). The support of the K3 camera is courtesy of Gatan, Inc.

Conflict of Interest

The authors declare no conflict of interest.

Keywords

2D materials, adventitious carbon, hydrogen evolution reaction (HER), monolayer MoS_2, pit formation, thermal oxidation

Received: May 4, 2020
Revised: June 26, 2020
Published online: August 2, 2020

[1] H. Zhu, X. Qin, L. Cheng, A. Azcatl, J. Kim, R. M. Wallace, *ACS Appl. Mater. Interfaces* **2016**, *8*, 19119.
[2] M. Yamamoto, T. L. Einstein, M. S. Fuhrer, W. G. Cullen, *J. Phys. Chem. C* **2013**, *117*, 25643.
[3] H. Zhou, F. Yu, Y. Liu, X. Zou, C. Cong, C. Qiu, T. Yu, Z. Yan, X. Shen, L. Sun, B. I. Yakobson, J. M. Tour, *Nano Res.* **2013**, *6*, 703.
[4] W. L. Spychalski, M. Pisarek, R. Szoszkiewicz, *J. Phys. Chem. C* **2017**, *121*, 26027.
[5] B. Zhao, C. Shang, N. Qi, Z. Y. Chen, Z. Q. Chen, *Appl. Surf. Sci.* **2017**, *412*, 385.
[6] H. Liu, N. Han, J. Zhao, *RSC Adv.* **2015**, *5*, 17572.
[7] Z. Wang, Q. Li, H. Xu, C. Dahl-Petersen, Q. Yang, D. Cheng, D. Cao, F. Besenbacher, J. V. Lauritsen, S. Helveg, M. Dong, *Nano Energy* **2018**, *49*, 634.
[8] J. Gao, B. Li, J. Tan, P. Chow, T. M. Lu, N. Koratkar, *ACS Nano* **2016**, *10*, 2628.
[9] D. Guo, R. Shibuya, C. Akiba, S. Saji, T. Kondo, J. Nakamura, *Science* **2016**, *351*, 361.
[10] L. Tao, Q. Wang, S. Dou, Z. Ma, J. Huo, S. Wang, L. Dai, *Chem. Commun.* **2016**, *52*, 2764.
[11] P. G. Collins, K. Bradley, M. Ishigami, A. Zettl, *Science* **2000**, *287*, 1801.
[12] M. K. Kostov, E. E. Santiso, A. M. George, K. E. Gubbins, M. B. Nardelli, *Phys. Rev. Lett.* **2005**, *95*, 136105.
[13] M.-S. Chou, J.-H. Chiou, *J. Environ. Eng.* **1997**, *123*, 437.
[14] Y. C. Lin, D. O. Dumcenco, Y. S. Huang, K. Suenaga, *Nat. Nanotechnol.* **2014**, *9*, 391.
[15] S. Wang, Z. Qin, G. S. Jung, F. J. Martin-Martinez, K. Zhang, M. J. Buehler, J. H. Warner, *ACS Nano* **2016**, *10*, 9831.
[16] Q. Chen, H. Li, S. Zhou, W. Xu, J. Chen, H. Sawada, C. S. Allen, A. I. Kirkland, J. C. Grossman, J. H. Warner, *ACS Nano* **2018**, *12*, 7721.
[17] Y. C. Lin, D. O. Dumcenco, H. P. Komsa, Y. Niimi, A. V. Krasheninnikov, Y. S. Huang, K. Suenaga, *Adv. Mater.* **2014**, *26*, 2857.
[18] S. Wang, G. D. Lee, S. Lee, E. Yoon, J. H. Warner, *ACS Nano* **2016**, *10*, 5419.
[19] J. C. Matsubu, S. Zhang, L. DeRita, N. S. Marinkovic, J. G. Chen, G. W. Graham, X. Pan, P. Christopher, *Nat. Chem.* **2017**, *9*, 120.
[20] S. F. Tan, S. W. Chee, Z. Baraissov, H. Jin, T. L. Tan, U. Mirsaidov, *Adv. Funct. Mater.* **2019**, *29*, 1903242.
[21] L. Zou, J. Li, D. Zakharov, E. A. Stach, G. Zhou, *Nat. Commun.* **2017**, *8*, 307.
[22] B. Radisavljevic, A. Radenovic, J. Brivio, V. Giacometti, A. Kis, *Nat. Nanotechnol.* **2011**, *6*, 147.
[23] R. Sinclair, P. J. Kempen, R. Chin, A. L. Koh, *Adv. Eng. Mater.* **2014**, *16*, 476.
[24] E. D. Boyes, P. L. Gai, *Ultramicroscopy* **1997**, *67*, 219.
[25] I. Song, C. Park, M. Hong, J. Baik, H. J. Shin, H. C. Choi, *Angew. Chem., Int. Ed.* **2014**, *53*, 1266.
[26] J. Miao, F.-X. Xiao, H. B. Yang, S. Y. Khoo, J. Chen, Z. Fan, Y.-Y. Hsu, H. M. Chen, H. Zhang, B. Liu, *Sci. Adv.* **2015**, *1*, e1500259.
[27] M. V. Bollinger, K. W. Jacobsen, J. K. Nørskov, *Phys. Rev. B* **2003**, *67*, 129906.
[28] A. M. van der Zande, P. Y. Huang, D. A. Chenet, T. C. Berkelbach, Y. You, G. H. Lee, T. F. Heinz, D. R. Reichman, D. A. Muller, J. C. Hone, *Nat. Mater.* **2013**, *12*, 554.
[29] C. Tsai, H. Li, S. Park, J. Park, H. S. Han, J. K. Norskov, X. Zheng, F. Abild-Pedersen, *Nat. Commun.* **2017**, *8*, 15113.
[30] J. Cheng, T. Jiang, Q. Ji, Y. Zhang, Z. Li, Y. Shan, Y. Zhang, X. Gong, W. Liu, S. Wu, *Adv. Mater.* **2015**, *27*, 4069.
[31] S. Najmaei, Z. Liu, W. Zhou, X. Zou, G. Shi, S. Lei, B. I. Yakobson, J. C. Idrobo, P. M. Ajayan, J. Lou, *Nat. Mater.* **2013**, *12*, 754.
[32] L. Cai, C. J. McClellan, A. L. Koh, H. Li, E. Yalon, E. Pop, X. Zheng, *Nano Lett.* **2017**, *17*, 3854.

[33] T. F. Jaramillo, K. P. Jorgensen, J. Bonde, J. H. Nielsen, S. Horch, I. Chorkendorff, *Science* **2007**, *317*, 100.
[34] J. Feng, M. Graf, K. Liu, D. Ovchinnikov, D. Dumcenco, M. Heiranian, V. Nandigana, N. R. Aluru, A. Kis, A. Radenovic, *Nature* **2016**, *536*, 197.
[35] X. Duan, C. Wang, J. C. Shaw, R. Cheng, Y. Chen, H. Li, X. Wu, Y. Tang, Q. Zhang, A. Pan, J. Jiang, R. Yu, Y. Huang, X. Duan, *Nat. Nanotechnol.* **2014**, *9*, 1024.
[36] J. Feng, K. Liu, R. D. Bulushev, S. Khlybov, D. Dumcenco, A. Kis, A. Radenovic, *Nat. Nanotechnol.* **2015**, *10*, 1070.